Sensitivity improvement of TiO$_2$-doped SnO$_2$ to volatile organic compounds

Wen Zeng [a,b], Tianmo Liu [a,**], Zhongchang Wang [b,*]

[a] College of Materials Science and Engineering, Chongqing University, Chongqing 400030, PR China
[b] World Premier International Research Center, Advanced Institute for Materials Research, Tohoku University, 2-1-1 Katahira, Aoba-ku, Sendai 980-8577, Japan

ARTICLE INFO

ABSTRACT

Most of volatile organic compounds (VOCs) are often harmful or even toxic for environment, which require in situ detection. Here, we demonstrate that the TiO$_2$ additive can enhance significantly gas-sensing properties of the SnO$_2$-based sensor to VOCs, independent of its content and the concentration of tested gases. The improved gas-sensing quantities of matter, i.e., maximum sensitivity, minimum gas concentration, optimal operating temperature, and response and recovery times, are found to satisfy the basic needs for a practical application, which renders the TiO$_2$–SnO$_2$ composite material promising for the development of sensor devices to VOCs.

© 2010 Elsevier B.V. All rights reserved.

1. Introduction

One of the most active fields in the sensor research is the exploration of new materials that enable enhanced gas-sensing properties. Of all the materials currently examined, semiconducting oxides, for example, SnO$_2$ and TiO$_2$, are of strong interest, largely because their physical properties are important for promising application as a gas sensor [1–4]. Although the two dioxides have a number of intrinsic properties in common, the philosophies behind their gas-detection behaviors differ from each other remarkably. The gas-sensing property for the SnO$_2$-based sensors is found to be affected dominantly or even controlled by their surfaces, while that for the TiO$_2$-based sensors by their bulk constituents as well [5,6]. As a consequence of this fundamental difference, the SnO$_2$-based sensors are capable of being operated at moderate temperatures (e.g., 573–673 K), whereas TiO$_2$-based sensors are suited to work at high temperatures (e.g., 1273–1473 K) because the TiO$_2$ has a far higher resistance than the SnO$_2$ [7–9].

Since the two oxides have distinct gas-sensing behaviors, a combination of them would presumably initiate a new system, which might have the properties that are not present in either of their bulk oxides. One typical example is that the TiO$_2$ doping is well known to enhance the gas-sensing function of either WO$_3$-based or ZnO$_2$-based sensors [10–12]. However, it yet remains unknown whether the TiO$_2$ doping can alter or improve the gas-sensing performance of SnO$_2$, one of the most important materials for sensor devices. A clarification of this point would not only add further understanding toward the gas-sensing origin but

also open up a new avenue for seeking novel materials that can optimize sensing characteristics of the commonly used SnO$_2$. Here, we investigate the doping effect of TiO$_2$ on microstructure evolution and sensing property of SnO$_2$ to volatile organic compounds (VOCs) such as methanol, ethanol, formaldehyde, and acetone. We have chosen the VOCs deliberately because most of them are very harmful to environment, which are necessary to be detected once they are produced. In addition, there are still no simple and practical electronic sensors available for the in situ monitoring of these gases. Our results show that the TiO$_2$ is eligible for improving the response of SnO$_2$ to VOCs dramatically, thereby holding the technological promise for a VOC sensor.

2. Experimental

Colloidal solution of TiO$_2$ was prepared by first mixing 10 mL tetrabutyl titanium (Wako Pure Chemical, 95%) with 4 mL isopropyl alcohol, which was then added gradually to 150 mL distilled water under stirring for several hours till sol was formed. The sol was subsequently transferred to a well sealed autoclave vessel that contains 0.5 M teramethyl ammonium hydroxide. Finally, the solution was peptized via a heat treatment at 393 K for 6 h. As for the preparation of SnO$_2$ colloidal solution, the SnCl$_4 \cdot 5$H$_2$O (Wako Pure Chemical, 95%) was first dissolved in 0.4 M ethanol, and then the solution was stirred and refluxed for 3 h. Further, aqueous ammonia of 5.5 M (Wako Pure Chemical, 25 − 27.9%) was introduced dropwise into the refluxed solution, forming precipitates. The resultant precipitate was finally washed thoroughly and diluted by deionized water to form the SnO$_2$ colloidal solution.

The SnO$_2$–TiO$_2$ composite was prepared by simply mixing the TiO$_2$ with the SnO$_2$ colloidal solution under a variety of mass ratios.

* Corresponding author. Tel.: +81 22 217 5933; fax: +81 22 217 5930.
** Also corresponding author.
E-mail addresses: tmliu@cqu.edu.cn (T. Liu),
zcwang@wpi-aimr.tohoku.ac.jp (Z. Wang).

The mixed solution was desiccated to gel, grinded to powder, and annealed at 723 K in air for 2 h. The SnO$_2$–TiO$_2$ paste was fabricated by adding ethanol to the solution, followed by the coating of the mixture on an Al$_2$O$_3$ tube that has attached two Au electrode wires in advance. The ceramic tube was further sintered at 573 K in air for 2 h. It was worthy of mentioning that a Ni–Cr alloy coil was placed in the tube in order to adjust output of the heating power.

Microstructure characterization was performed using X-ray diffraction (XRD). A Shimadzu XD-5A diffractometry with the Cu Kα radiation operated at 30 kV and 100 mA was applied. Surface morphologies for both the pristine and doped samples were observed using a JEOL JSM-5510 scanning electron microscope (SEM) and a contact mode CSPM4000 atomic force microscope (AFM). After the sensor was powered at 373 K in air for 120 h, the gas-sensing property was measured by a static system controlled by a computer under the laboratory conditions, namely, 303 K and relative humidity of 40%. In this work, the gas response was defined as the ratio of resistance (R_0) in air to that in gas (R).

3. Results and discussion

3.1. Characterization of SnO$_2$–TiO$_2$ composite materials

To determine the chemical composition of the sintered powder, we performed the XRD analyses, as shown in Fig. 1, where textual orientations of the detected matters are labeled as well for easy reference. From Fig. 1(a), only the SnO$_2$ peaks can be observed for the undoped sample, as expected from the preparation process described above. In addition, the pristine SnO$_2$ is found to have a rutile phase with multiple orientations, among which the (1 1 0) grain has the highest concentration, as estimated from the strongest intensity of its diffraction peak (Fig. 1(a)). Not surprisingly, the TiO$_2$ peaks emerge in the XRD patterns after doping, meaning that we have successfully incorporated TiO$_2$ into SnO$_2$. From Fig. 1(b)−(e), the added TiO$_2$ is found to have an anatase phase with mainly (1 0 1) textures, where their peak intensities become stronger with the rise of doped TiO$_2$. In addition to the (1 0 1) orientations, the (2 0 0) textures are also identified in all the doped samples, although their amount is comparatively smaller. Finally, we notice that there appears no diffraction peak for any other unwanted compounds such as Ti$_x$Sn$_{1−x}$O$_2$ in the XRD patterns of the doped samples, meaning that the doped sample can be viewed
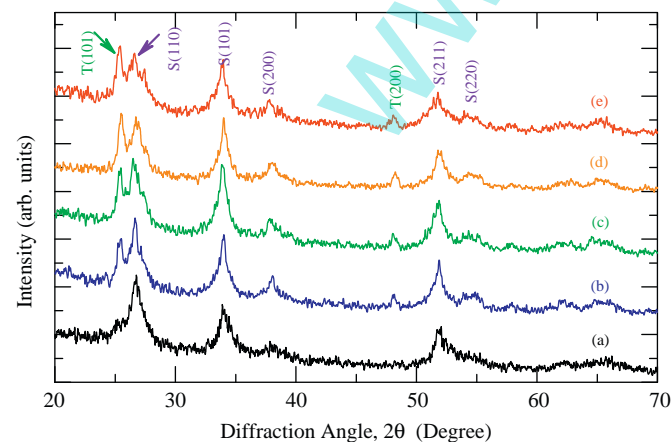
as a simple agglomeration of TiO$_2$ with SnO$_2$ particles. Further, this agrees well with other experimental reports [13,14].

The Scherrer equation [15], which addresses a quantitative relation between the mean particle size (D) and the full-width at high-maximum of XRD peaks (β), can be expressed by $D = 0.89\lambda/(\beta \cos\theta)$, where θ is Bragg angle and λ is X-ray wavelength (Cu Kα, 0.154 nm). In light of this formula, the average particle size of the pristine SnO$_2$ is estimated to be 25 nm, while those of the SnO$_2$ under doping concentrations of 0.1, 0.3, 0.5, and 0.8 to be 20, 16, 13, and 10 nm, respectively. Evidently, the grains in the SnO$_2$ are refined as the amount of doped TiO$_2$ increases, which can be understood by considering that the doped TiO$_2$ may diffuse into the grain boundaries of the polycrystalline SnO$_2$, thereby preventing the grains from growing.

To characterize the surface morphology and confirm the grain refinement after doping, we further performed SEM and AFM observations on the pristine and TiO$_2$-doped SnO$_2$ with a Ti/Sn ratio of 0.5 after annealing at 723 K for 2 h (Fig. 2). From the SEM images (Fig. 2(a) and (c)), the surface morphologies in both cases are observed to be very rough with the presence of a large amount of grain agglomeration. This rough surface can be confirmed in the AFM images (Fig. 2(b) and (d)) showing many visible islands. Moreover, comparing the SEM image of the pristine sample (Fig. 2(a)) with that of the doped sample (Fig. 2(c)), we note qualitatively that the grains are indeed refined after doping TiO$_2$, which agrees with the above XRD results. Since smaller grains generally result in higher specific surface area, this structural optimization may play an important role in altering or improving gas-sensing property of TiO$_2$-doped SnO$_2$ sensors.

3.2. Gas-sensing properties

In support of this idea, we first present in Fig. 3, the response to several VOC gases, methanol, ethanol, formaldehyde, and acetone, at a variety of operating temperatures. From this figure, one can clearly see that the response changes remarkably with the temperature. A common feature is that as temperature elevates, the response increases initially but undergoes a subsequent decrease, thereby passing through a maximum at the optimal operating temperature. The optimal temperatures for the sensors to formaldehyde and acetone are the same (633 K), which are somewhat larger than those of 553 and 613 K in the ethanol and methanol cases. In addition, we note that the response of doped SnO$_2$ is always larger than that of the pristine SnO$_2$, regardless of the gas species introduced, suggesting an improvement of the sensing property to the VOCs via doping. However, the response increases only slightly as the doped TiO$_2$ increases. The sensitivity enhancement through the TiO$_2$ doping can be understood by considering that (i) electrons are given out when the pre-absorbed oxygen reacts with the VOCs, as can be described by the chemical reactions, $\text{VOCs} + \text{O}^- \rightarrow \text{VOCs} - \text{O} + e^-$ and $\text{VOCs} + \text{O}^{2-} \rightarrow \text{VOCs} - \text{O} + 2e^-$ and (ii) the TiO$_2$ additive refines the grains in SnO$_2$, which may be important for facilitating the oxygen adsorption, although further studies are required to develop a general knowledge on the underlying origin.

To further investigate how the gas concentration affects the response, we present in Fig. 4 sensitivity to methanol, ethanol, formaldehyde, and acetone. Independent of the gas species and mass ratio of Ti/Sn, the sensitivity increases dramatically with no sign of saturation, as the concentration ranges from 50 to 400 ppm. In addition, we note that the curves in all cases are nearly linear, indicative of strong dependence of sensitivity on gas concentration. It is worthy of mentioning that the sensitivity in either the formaldehyde or acetone case has already exceeded a threshold value (20) under the concentration of 50 ppm, which meets the

Fig. 1. X-ray diffraction patterns of the composite powders sintered at 723 K for 2 h. The TiO$_2$ was introduced into the SnO$_2$ under various concentrations: (a) SnO$_2$, (b) Ti/Sn = 0.1, (c) Ti/Sn = 0.3, (d) Ti/Sn = 0.5, and (e) Ti/Sn = 0.8. Note that the T and S represent TiO$_2$ and SnO$_2$, respectively.
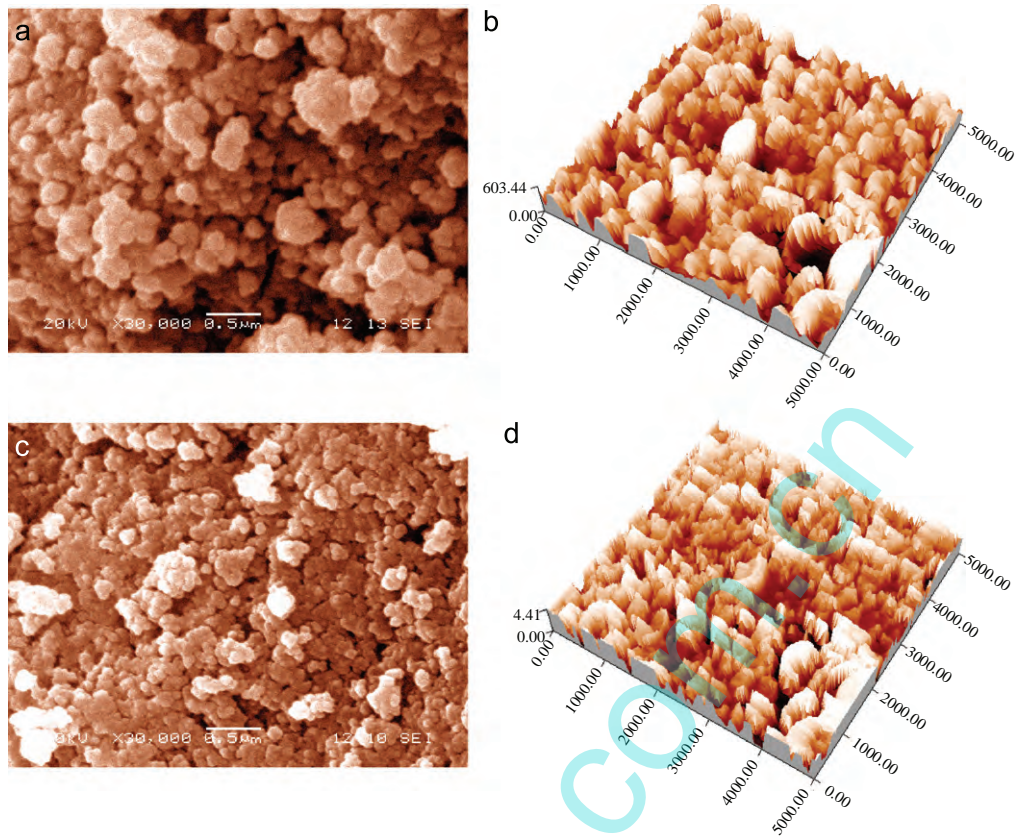
Fig. 2. (a) SEM and (b) AFM images of pristine SnO_2 surface after annealing at 723 K for 2 h. (c) SEM and (d) AFM images of surface of TiO_2–SnO_2 with Ti/Sn=0.5.
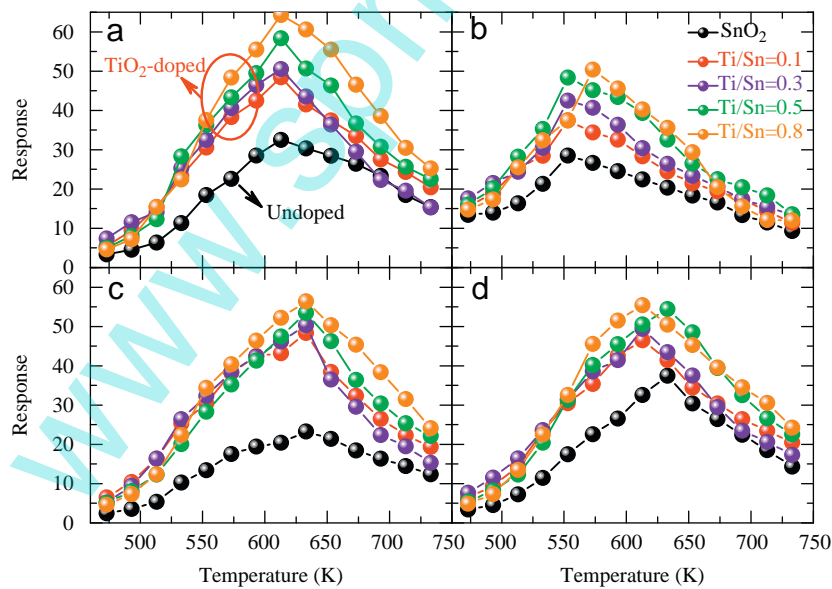
Fig. 3. Variation in response as a function of operating temperature for the sensors to (a) methanol, (b) ethanol, (c) formaldehyde, and (d) acetone under a concentration of 200 ppm.

demands for practical application. Moreover, the sensitivity is observed to behave differently for each VOC gas, which may be attributable to their varying chemical characteristics. Compared to the pristine SnO_2, the TiO_2-doped SnO_2 shows a larger sensitivity to VOC gases even when the gas concentration is low, which implies that TiO_2-doped SnO_2 composite is promising for developing a sensor device that can monitor air quality.

Fig. 5 shows typical response-recovery characteristics for the TiO_2-doped SnO_2 sensor under a gas concentration of 200 ppm, where one can see that the voltage in all cases increases abruptly after the introduction of gas, but returns to original state after releasing the gas. Evidently, the curves differ from one another, indicative of the strong dependence of response and recovery times on gas species. Of all types of gas, the methanol exhibits the highest
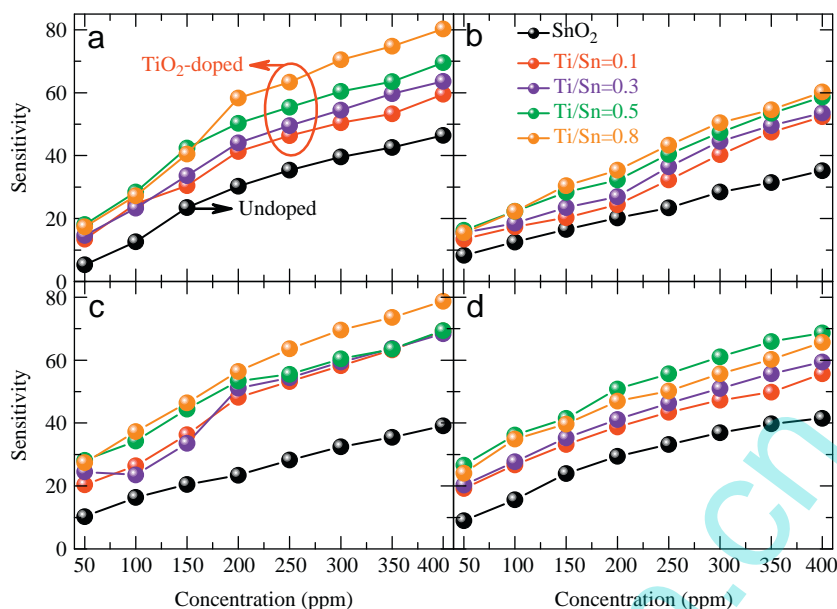
Fig. 4. Dependence of sensitivity on concentration for the sensors to (a) methanol, (b) ethanol, (c) formaldehyde, and (d) acetone under an operating temperature of 633 K.
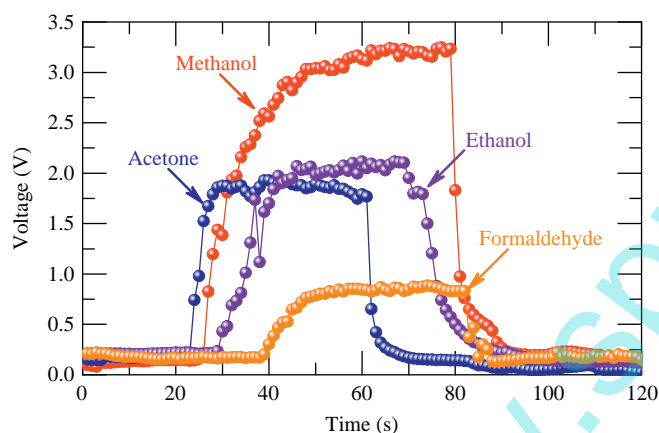
Fig. 5. Response-recovery characteristics for the SnO_2–TiO_2 sensor with Ti/Sn=0.8 operated at 633 K under a concentration of 200 ppm for each type of gas.

Fig. 6. Schematic plot illustrating the possible transition from coupled TiO_2/SnO_2 to TiO_2–SnO_2 composites.

response at the operating stage, which means that the TiO_2-doped SnO_2 is a potential material for detecting methanol. Since, in general, the response and recovery time can be defined as the time needed to reach 90% response (recovery) when gas is in (out), here the response and recovery times for all sensors are estimated to be 10–15 and 14–20 s, respectively, which meet the basic needs for an industrial application.

3.3. Gas-sensing mechanism of the TiO_2–SnO_2 system

Although a number of works have been conducted on the SnO_2-based sensors, its mechanism remains controversial. The current understanding of its gas-sensing origin, which is mainly based on trial-and-error test and conjecture, can be summarized in three major points: (1) sensing property of SnO_2-based sensor is governed by surfaces [16], (2) the resistance change (i.e., response) is controlled by the species and amount of chemisorbed oxygen on the surface of sensor [16–18], (3) pre-adsorbed oxygen can gain electrons from the surface, producing various forms of oxygen ions,

as can be expressed by $O_2(gas) \rightarrow O_2(ads)$, $O_2(ads)+e^- \rightarrow O_2^-(ads)$, and $O_2^-(ads)+e^- \rightarrow 2O^-(ads)$ [19–21]. The results presented here demonstrate that no solid solution, namely, substitution of Sn by Ti, is present [14,16], in stark contrast to the report by Radecka et al., which is mainly because the solution formation temperature in their case (1723 K) is far higher than the annealing temperature we used (723 K) [8]. In this sense, the TiO_2–SnO_2 mixed system prepared by the sol-gel method can be simply viewed as a couple of anatase TiO_2 with rutile SnO_2 grains (Fig. 6) [16].

Fig. 7 illustrates the change of energy band during gas sensing. As seen in Fig. 7(a)−(c), the pre-adsorbed oxygen could give rise to a depletion layer near to the surface of n-type semiconducting oxides [18], which results in a band bending around surface. This band bending inclines to increase the energy barrier and hence resistance of composite [22,23]. On the other hand, there may appear noticeable charge transfer from the TiO_2 to SnO_2 because both the conduction band (CB) minimum and valence band (VB) maximum of TiO_2 are larger than those of SnO_2 (Fig. 7(d) and (e)). Since the SnO_2 has a high work function and the TiO_2 is of a strong electron affinity [24–27], the hetero-junctions may emerge at grain boundaries and maintain till the electron affinity of adsorbed oxygen reaches the same level as that of TiO_2–SnO_2. This can, therefore, facilitate the oxygen adsorption on the surface.

Due to the strong electron negativity of the adsorbed oxygen, they may act as traps for CB electrons and can therefore deteriorate electric conductivity through the oxide. As the reductive gas, for example, ethanol, is introduced (Fig. 8), chemical reactions would
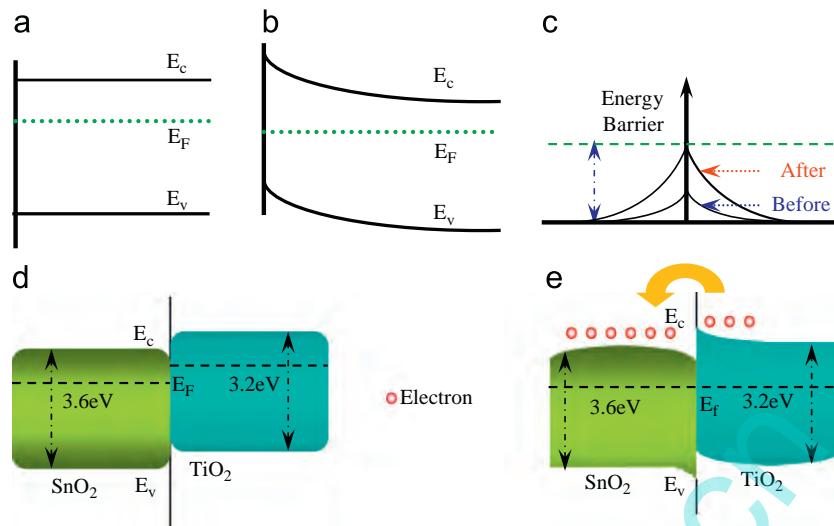
Fig. 7. Energy-band diagram for the TiO$_2$–SnO$_2$ composite system (a) before and (b) after oxygen adsorption. (c) Change in energy barrier induced by oxygen adsorption. Energy band for the composite system (d) before and (e) after the contact of SnO$_2$ to TiO$_2$.
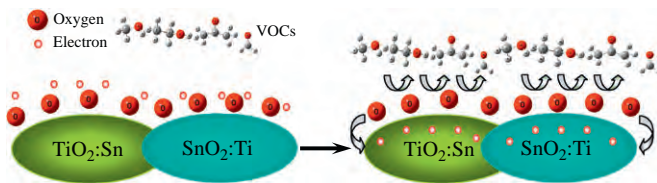
Fig. 8. Schematic of an electron transfer process on the surface of TiO$_2$–SnO$_2$.
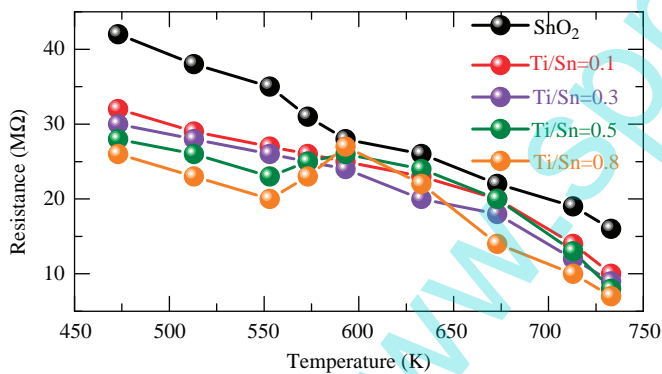
Fig. 9. Correlation between resistance and operating temperature for the TiO$_2$–SnO$_2$ samples with different Ti/Sn ratios.

take place between ethanol molecule and the pre-adsorbed oxygen on the composite surface, as described in the following equations [28,29]:

$$C_2H_5OH(gas)+O^{2-}(ads) \rightarrow C_2H_5O^-(gas)+OH^-(ads),$$

$$C_2H_5O^-(gas) \rightarrow (C_2H_5)_2O(ads)+O^-(ads)+e^-,$$

$$2C_2H_5OH(gas)+O^{2-}(ads) \rightarrow 2C_2H_4O^-(ads)+2H_2O,$$

$$C_2H_4O^-(ads) \rightarrow CH_3CHO(ads)+e^-,$$

$$CH_3CHO(ads)+5O^{2-}(ads) \rightarrow 4CO_2+4H_2O+10e^-.$$
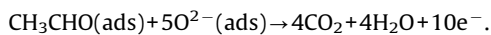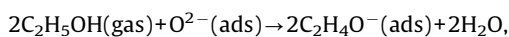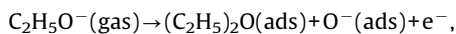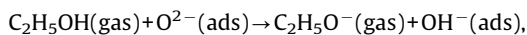
The high density of electrons produced by the above reactions may lower, to a large extent, the resistance of oxide and can therefore

result in an abrupt increase of output voltage, as generally observed at the operating stage of the SnO$_2$-based sensor (Fig. 5) [30].

To confirm the effect of adsorbed oxygen on gas-sensing properties, we finally investigate the change of resistance as a function of operating temperature, as shown in Fig. 9. We note first that resistance reduces gradually from 473 to 553 K, which can be attributed to the following two competitive processes [11,30]: (i) the conductance of oxide increases with the rise of operating temperature owing to intrinsic excitation, and (ii) adsorbed oxygen gains electrons from the oxide surface, which deteriorates electron transport across the surface. Interestingly, as the temperature is elevated from 553 to 593 K, the resistance of highly doped samples (Ti/Sn=0.5 and 0.8) increases, which implies that the amount of oxygen absorbed is more significant for heavier doping. However, when temperature is beyond 593 K, the resistances in all samples decrease, inferring that the intrinsic excitation dominates at high temperature. In comparison to the TiO$_2$-doped case, the resistance in the undoped case is somewhat larger with the rise of temperature, which indicates that the doped sample is capable of capturing more oxygen. This, together with the remarkable difference in the response to VOCs for the samples with the different Ti/Sn ratios, suggests that pre-adsorbed oxygen is crucial to improve the gas-sensing property of TiO$_2$–SnO$_2$.

4. Conclusion

We have incorporated TiO$_2$ into SnO$_2$ and investigated the microstructures and gas-sensing properties of SnO$_2$–TiO$_2$ sensors, taking into account the effects of content and gas concentration of the TiO$_2$ additives. We have found that although no new chemical compound is formed, the doped TiO$_2$ can enhance the gas sensitivity of SnO$_2$ to tested VOC gases significantly, *regardless* of the operating temperature and gas concentration. Qualitatively, we attribute the improvement of sensitivity to VOCs to the noticeable grain refinement via doping and the potential facilitation of oxygen adsorption on the sensor surface. The response and recovery times are estimated to be 10–15 and 14–20 s, respectively, which meet basically industrial needs. The findings presented in this paper demonstrate that the TiO$_2$-doped SnO$_2$ may be a promising sensing material for the effective detection of VOCs.

Acknowledgements

References

[1] M. Hemissi, H. Amardjia-Adnani, J.C. Plenet, Curr. Appl. Phys. 9 (2009) 717.
[2] K. Shimanoe, K. Ikari, Y. Shimizd, N. Yamazoe, Sens. Actuators B 118 (2006) 90.
[3] C.V. Gopal Reddy, W. Cao, O.K. Tan, W. Zhu, Sens. Actuators B 81 (2002) 170.
[4] D.R. Zhang, Y.H. Kim, Y.S. Kang, Curr. Appl. Phys. 6 (2006) 801.
[5] M. Batzill, Sensors 6 (2006) 1345.
[6] O.K. Varghese, C.A. Grimes, J. Nanosci. Nanotech. 3 (2003) 277.
[7] F. Edelman, H. Hahn, S. Seifried, C. Alof, H. Hoche, A. Balogh, P. Werner, K. Zakrzewska, M. Radecka, P. Pasoerb, A. Chack, V. Mikhelashvili, G. Eisenstein, Mater. Sci. Eng. B 69−70 (2000) 386.
[8] M. Radecka, K. Zakrzewska, M. Rgkas, Sens. Actuators B 47 (1998) 194.
[9] C.M. Carney, S. Yoo, S.A. Akbar, Sens. Actuators B 108 (2005) 29.
[10] C.V. Gopal Reddy, W. Cao, O.K. Tan, W. Zhu, S.A. Akbar, Sens. Actuators B 94 (2003) 99.
[11] B.L. Zhu, C.S. Xie, W.Y. Wang, K.J. Huang, J.H. Hu, Mater. Lett. 58 (2004) 624.
[12] E. Comini, G. Sberveglieri, V. Guidi, Sens. Actuators B 70 (2000) 108.
[13] D. Garcia, D. Speidel, J. Am. Ceram. Soc. 55 (1972) 322.
[14] N.N. Padurow, Naturwissenschaften 43 (1956) 395.
[15] M. Bhagwat, P. Shah, V. Ramaswamy, Mater. Lett. 57 (2003) 1604.
[16] K. Zakrzewska, M. Radecka, Thin Solid Film 515 (2007) 8332.
[17] J. Shang, W. Yao, Y. Zhu, N. Wu, Appl. Catal. A 257 (2004) 25.
[18] H.C. Lee, W.S. Hwang, Mater. Trans. 46 (2005) 1942.
[19] Z.H. Jing, Mater. Sci. Eng. A 441 (2006) 176.
[20] X.H. Wu, Y.D. Wang, H.L. Liu, Y.F. Li, Z.L. Zhou, Mater. Lett. 56 (2002) 732.
[21] N. Yamazoe, G. Sakai, K. Shimanoe, Catal. Surv. Asia 7 (2003) 63.
[22] S.M. Sze, Semiconductor Sensors, John Wiley and Sons, New York, 1994, pp. 388–396.
[23] V. Lantto, T.S. Rantala, Sens. Actuators B 19 (1994) 711.
[24] C. Xiong, K.J. Balkus, J. Phys. Chem. C 111 (2007) 10359.
[25] Y. Shimizu, N. Kuwano, T. Hyodo, M. Egashira, Sens. Actuators B 83 (2002) 195.
[26] A.K. Prasad, D.J. Kubinski, P.I. Gouma, Sens. Actuators B 93 (2003) 25.
[27] M.H. Yeh, W.S. Hwang, G.B. Lee, Y.M. Lu, Mater. Trans. 45 (2004) 3318.
[28] X.F. Chu, X.Q. Liu, G.Z. Wang, G.G. Meng, Mater. Res. Bull. 34 (1999) 1789.
[29] J. Xu, J. Han, Y. Zhang, Y. Sun, B. Xie, Sens. Actuators B 132 (2008) 334.
[30] D.A. Neamen, Semiconductor Physics and Devices: Basic Principles, Second ed., IRRWIN, 1997, pp. 340−314.